Multi-User Digital Beamforming Based on Path Angle Information for mm-Wave MIMO Systems

Israa Khaled, Ammar El Falou, Charlotte Langlais, Bachar El Hassan, Michel Jezequel

Multi-User Digital Beamforming Based on Path Angle Information for mm-Wave MIMO Systems

Israa Khaled*†, Ammar El Falou*, Charlotte Langlais†, Bachar El Hassan*, Michel Jezequel†
* Lebanese University, Faculty of Engineering, Tripoli, Lebanon
† IMT Atlantique, Electronics Department, CNRS UMR 6285 Lab-STICC, Brest, France

***Abstract*—In millimeter-wave wireless communications, beamforming, also known as beamsteering is a promising technique that enables the base station, with a large number of antennas, to mitigate the tremendous path loss. This paper aims to assess the performance of two digital beamformers, namely, conjugate beamforming (CB) and digital beamsteering (DBS) in a millimeter-wave environment based on geometric aspects, such as the antenna array topology or the location of the user in the cell. The realistic channel model NYUSIM, from New York University, reproduces a mono- and multi-path urban scenario. We show that DBS, with only line-of-sight path angle information at the transmitter, outperforms CB, with full channel state information at the transmitter, in mono-path environment. However, in multi-path scenario, DBS is not able to exploit the diversity of non-line-of-sight paths and CB outperforms DBS.**

***Index Terms*—Beamforming, multi-user, MIMO, millimeter-wave, antenna array.**

I. Introduction

The demands of cellular data traffic grow faster and faster in addition to the appearance of bandwidth-hungry applications [1], [2]. The spectrum below 6-GHz is already congested and the available bandwidth is not sufficient to fulfill these requirements. Subsequently, the next generation of wireless communication systems migrates toward the higher frequency bands - also known as millimeter-wave (mmWave) bands - with large chunks of wide bandwidth available to achieve high data rates [1], [3].

Massive multiple-input multiple-output (m-MIMO) can further boost the spectrum efficiency, by extensively exploiting the spatial diversity coming from the employment of massive antennas (dozens or hundreds) [2], [3]. With the tiny wavelength of those frequencies, massive antenna elements can be packed within a small form factor. Moreover, they provide an adequate spatial gain to overcome the severe mmWave path loss [4]. Therefore, beamforming (BF) with high-directional array is investigated as an appealing technique in mmWave wireless system [4], [5].

Digital BF (DBF) techniques are widely adopted for single-user and multi-user systems. However, implementing m-MIMO with fully DBF at mmWave frequencies poses many challenging issues: energy consumption, complexity and cost [4]. Recently, to overcome the high energy consumption of the front ends of mmWave system, solutions as low resolution digital-to-analog converters have been proposed in [6].

In this paper, we focus on the reduction of the complexity, by using a constant-envelope precoder, known as digital beamsteering (DBS) [7]. Based on a geometric partial channel state information at the transmitter (CSIT), mainly the angle of the line-of-sight (LOS) path and using only digital phase shifters, DBS forms and steers a beam toward the desired user. Unlike prior work that adopts a simplified mmWave channel model [7], the realistic channel model NYUSIM from New York University is considered in an urban scenario [8]–[10]. It also provides 2D and 3D channel models using different antenna array configurations (AACs), namely uniform linear array (ULA) and uniform planar array (UPA). As a reference, we consider conjugate beamforming (CB) that maximizes the BF gain at the desired user, based on full CSIT [11], [12]. Performance is assessed in terms of sum-rate. 2D spatial representations of beams, user paths and locations for some realizations illustrate the performance results.

The rest of the paper is structured as follows. Section II introduces the system model. Section III presents the derivations of sum-rate in mono- and multi-path environments. Section IV provides the numerical results in terms of sum-rates for CB and DBS with NYUSIM channel simulator. Finally, Section V concludes the paper .

We use the following notations: $\mathbf{A}$ is a matrix, $\mathbf{a}$ is a vector, a is a scalar, $(.)^T$ and $(.)^H$ stand for the transpose and the Hermitian transpose, respectively. $\mathbf{A} \otimes \mathbf{B}$ is the Kronecker product of $\mathbf{A}$ and $\mathbf{B}$. $\mathcal{N}(\mu, \sigma^2)$ denotes a Gaussian random vector with mean μ and variance σ^2. $\mathbf{A}_(i, j)$ is the (i, j)-th entry of $\mathbf{A}$ in the i-th row and j-th column.

II. System Model

We consider a mmWave m-MU-MIMO system, where a base station (BS) with $M = M_H \times M_V$ transmit antennas serves K single-antenna user equipments (UEs). M_H and M_V denote the number of horizontal and vertical BS antennas. Moreover, we assume that $K < M$, generally considered in m-MIMO systems.

BS applies a fully digital beamforming $\mathbf{W} \in \mathbb{C}^{M \times K}$, and thereby the received signal $\mathbf{y} \in \mathbb{C}^{K \times 1}$ can be defined as:

$$\mathbf{y} = \sqrt{\eta}\mathbf{H}\mathbf{W}\mathbf{s} + \mathbf{n} = \mathbf{H}\mathbf{W}_n\mathbf{s} + \mathbf{n} \tag{1}$$

where $\mathbf{s} \in \mathbb{C}^{K \times 1}$ contains the data symbol of all UEs, $\mathbf{H} = \begin{bmatrix}\mathbf{h}_1^T & \mathbf{h}_2^T \cdots & \mathbf{h}_K^T\end{bmatrix}^T \in \mathbb{C}^{K \times M}$ is the MU-MIMO channel matrix, $\mathbf{n} \in \mathbb{C}^{K \times 1}$ is the additive white Gaussian noise with $\mathbf{n} \sim \mathcal{N}(0, \sigma_n^2)$ and $\eta = \frac{1}{\mathrm{Tr}(\mathbf{W}^H\mathbf{W})}$ is the normalization factor that eliminates the beamforming effect on the transmission power.

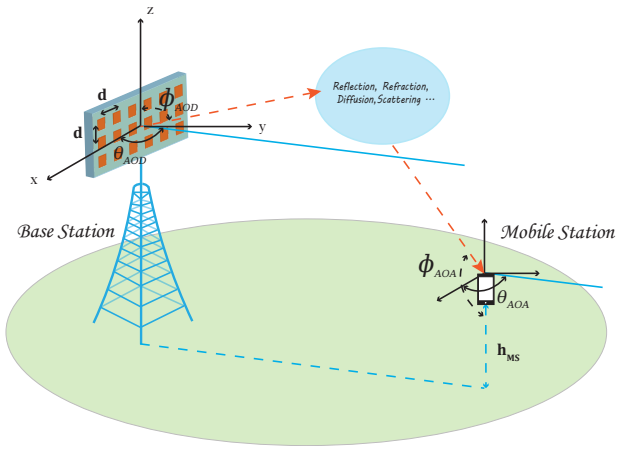

Fig. 1: Cell downlink MU-MIMO system.

We assume a narrowband multi-path channel for each UE. Thus, the channel $\mathbf{h}_k$ of the k-th UE (UE$_k$) is given by [13]:

$$\mathbf{h}_k = \sum_{n=1}^{N_k} \alpha_{k,n} e^{j\varphi_{k,n}} \mathbf{a}_R(\vec{\Phi}_{k,n}) \mathbf{a}_T^H(\vec{\Theta}_{k,n}) \tag{2}$$

where $\mathbf{a}_T$ and $\mathbf{a}_R$ denote the transmit and receive array steering vectors, N_k the number of paths in UE$_k$ channel, $\varphi_{k,n}$ and $\alpha_{k,n}$ the phase and the amplitude of the n-th path in UE$_k$ channel, $\vec{\Theta}_{k,n} = (\theta^t_{k,n}, \phi^t_{k,n})$ and $\vec{\Phi}_{k,n} = (\theta^r_{k,n}, \phi^r_{k,n})$ the vectors of azimuth and elevation angle of departure (AOD) and angle of arrival (AOA), respectively. All these parameters are generated by NYUSIM simulator. Note that the angles θ and ϕ in (x, y, z) are represented as shown in Fig. 1. We consider a far-field assumption and the use of omnidirectional antenna pattern.

As each UE has a single antenna, then $\mathbf{a}_R(\vec{\Phi}_{k,n}) = 1$. In the rest of this paper, we will use $\mathbf{a}_{k,n}$ instead of $\mathbf{a}_T(\vec{\Theta}_{k,n})$. Therefore, the channel vector $\mathbf{h}_k \in \mathbb{C}^{1\times M}$ can be given by:

$$\mathbf{h}_k = \sum_{n=1}^{N_k} \alpha_{k,n} e^{j\varphi_{k,n}} \mathbf{a}_{k,n}^H \tag{3}$$

A. 2-D and 3-D array steering vector

The transmit antenna array is characterized by the array steering vector $\mathbf{a}$.

When BS adopts a uniform linear antenna array, the channel model is represented in 2D and $\mathbf{a}(\vec{\Theta}) = \mathbf{a}(\theta) \in \mathbb{C}^{M\times 1}$ is a function of the angular direction θ of the plane wave. For an horizontal ULA array along x-axis, $\mathbf{a}(\theta)$ can be written as:

$$\mathbf{a}(\theta) = \left[1, e^{j2\pi \frac{d}{\lambda}\cos(\theta)}, \cdots, e^{j2\pi(M-1)\frac{d}{\lambda}\cos(\theta)}\right]^T \tag{4}$$

However, in 3D channel model with uniform planar array located in xoz plane, $\mathbf{a}(\theta, \phi) = \mathbf{a}_{\text{az}}(\theta, \phi) \otimes \mathbf{a}_{\text{el}}(\phi)$ is a function of azimuth angle θ and elevation angle ϕ with:

$$\mathbf{a}_{\text{az}}(\theta, \phi) = \left[1, e^{j2\pi \frac{d}{\lambda}\cos(\theta)\sin(\phi)}, \cdots, e^{j2\pi(M_H-1)\frac{d}{\lambda}\cos(\theta)\sin(\phi)}\right]^T \tag{5}$$

$$\mathbf{a}_{\text{el}}(\phi) = \left[1, e^{j2\pi \frac{d}{\lambda}\cos(\phi)}, \cdots, e^{j2\pi(M_V-1)\frac{d}{\lambda}\cos(\phi)}\right]^T \tag{6}$$

where d is the inter-element spacing distance and λ is the wavelength.

B. Fully digital beamforming

1) Conjugate beamforming (CB): CB maximizes the beamforming gain at the intended UE, using full CSIT. The CB beamformer is given by [12]:

$$\mathbf{W}^{CB} = \mathbf{H}^H \tag{7}$$

The precoder envelope depends on $\mathbf{H}$. This directly impacts the peak-to-average power ratio (PAPR) of the waveform. Moreover, CB needs instantaneous full CSIT, i.e. the channel matrix $\mathbf{H}$. This will impact the rate of feedback link.

2) Digital beamsteering (DBS): DBS forms and steers a beam toward the intended UE using digital phase shifters. The DBS beamformer is based on the steering matrix $\mathbf{A} \in \mathbb{C}^{M\times K}$ corresponding to the LOS path, i.e., the path with highest power, labeled by $n = 1$ [7]:

$$\mathbf{W}^{DBS} = \mathbf{A}_{LOS} \tag{8}$$

$$\mathbf{A} = \begin{bmatrix} \mathbf{a}_{1,1} & \mathbf{a}_{2,1} & \cdots & \mathbf{a}_{K,1} \end{bmatrix} \tag{9}$$

The precoder envelope is constant. Thus, the PAPR is minimized and the energy efficiency of the amplifier is optimized. DBS is only based on the angle information of the LOS path of UE$_k$, i.e., $\vec{\Theta}_{k,1}$. This angle can be estimated using different beam-training strategies. This clearly shows that DBS needs less feedback rate than CB.

III. Sum-rate in mono- and multi-path environment

The sum-rate R_T is adopted as the performance metric in our work and is calculated as:

$$R_T = \sum_{k=1}^{K} R_k = \sum_{k=1}^{K} \log_2(1 + \text{SINR}_k) \tag{10}$$

where R_k and SINR$_k$ are the rate and the signal-to-interference-plus-noise ratio achieved at UE$_k$, respectively.

$$R_T = \sum_{k=1}^{K} \log_2 \left(1 + \frac{|\sqrt{\eta}(\mathbf{HW})_{(k,k)}|^2}{\sum\limits_{\substack{u=1 \\ u\neq k}}^{K} |\sqrt{\eta}(\mathbf{HW})_{(k,u)}|^2 + \sigma_n^2} \right) \tag{11}$$

A. Mono-path environment

Since one line-of-sight (LOS) path exists, we will use α_k, φ_k and $\mathbf{a}_k$ $\forall k \in \{1, ..., K\}$ instead of $\alpha_{k,1}$, $\varphi_{k,1}$ and $\mathbf{a}_{k,1}$. Thus, (3) can be expressed as: $\mathbf{h}_k = \alpha_k e^{j\varphi_k} \mathbf{a}_k^H$.

The DBS and CB beamforming matrix will be written as:

$$\mathbf{W}^{DBS} = \begin{bmatrix} \mathbf{a}_1 & \cdots & \mathbf{a}_K \end{bmatrix} \tag{12}$$

$$\mathbf{W}^{CB} = \begin{bmatrix} \alpha_1 e^{-j\varphi_1} \mathbf{a}_1 & \cdots & \alpha_K e^{-j\varphi_K} \mathbf{a}_K \end{bmatrix} \tag{13}$$

In mono-path environment, DBS generates a directional beam toward the intended UE with uniformly distributed power among all UEs. However, CB forms a directional beam toward

each UE with different power allocation and phase shift, based on their channel gains. In other words, the beam steered to the strongest UE (i.e., with the strongest channel gain) carries the greatest beamforming power.

SINR_k^{DBS} can be written as:

$$\text{SINR}_k^{DBS} = \frac{\eta^{DBS}\alpha_k^2|\mathbf{a}_k^H\mathbf{a}_k|^2}{\sum_{u=1,u\neq k}^{K}\eta^{DBS}\alpha_k^2|\mathbf{a}_k^H\mathbf{a}_u|^2+\sigma_n^2} \tag{14}$$

$$\text{SINR}_k^{DBS} = \frac{|\mathbf{a}_k^H\mathbf{a}_k|^2}{\sum_{u=1,u\neq k}^{K}|\mathbf{a}_k^H\mathbf{a}_u|^2+\frac{\sigma_n^2}{\eta^{DBS}\alpha_k^2}} \tag{15}$$

And, SINR_k^{CB} can be written as:

$$\text{SINR}_k^{CB} = \frac{\eta^{CB}\alpha_k^4|\mathbf{a}_k^H\mathbf{a}_k|^2}{\sum_{u=1,u\neq k}^{K}\eta^{CB}(\alpha_k\alpha_u)^2|\mathbf{a}_k^H\mathbf{a}_u|^2+\sigma_n^2} \tag{16}$$

$$\text{SINR}_k^{CB} = \frac{|\mathbf{a}_k^H\mathbf{a}_k|^2}{\sum_{u=1,u\neq k}^{K}\frac{\alpha_u^2}{\alpha_k^2}|\mathbf{a}_k^H\mathbf{a}_u|^2+\frac{\sigma_n^2}{\eta^{CB}\alpha_k^4}} \tag{17}$$

The interference factor $\beta_{k,u}$ is defined as $\beta_{k,u} = \mathbf{a}_k^H\mathbf{a}_u$. For CB and DBS, the interference at UE_k is caused by the beams generated toward other UEs (UE_u, $\forall u \neq k$), with $\vec{\Theta}_u$ close to $\vec{\Theta}_k$.

Moreover, for CB, this interference depends on $\frac{\alpha_u^2}{\alpha_k^2}$, as shown in (17). For instance, if UE_k has a strong channel gain and UE_u has a weak one, then $\frac{\alpha_u^2}{\alpha_k^2} < 1$ and UE_u has low interference impact on UE_k. In contrast, when applying DBS, the interference term does not depend on the channel gain of UEs, as shown in (15), and therefore the inter-user interference only depends on the proximity of $\vec{\Theta}_k$ and $\vec{\Theta}_u$, independently of their channel gain.

B. Multi-path environment

The DBS beamforming matrix is obtained based on the LOS path, labeled by $n = 1$ as:

$$\mathbf{W}^{DBS} = \mathbf{A} = \begin{bmatrix}\mathbf{a}_{1,1} & \mathbf{a}_{2,1} & \cdots & \mathbf{a}_{K,1}\end{bmatrix} \tag{18}$$

And, the beamforming matrix of CB can be written as:

$$\mathbf{W}^{CB} = \begin{bmatrix}\underbrace{\sum_{n=1}^{N_1}\alpha_{1,n}e^{-j\varphi_{1,n}}\mathbf{a}_{1,n}}_{\text{superposition of multiple beams}} & \cdots & \sum_{n=1}^{N_K}\alpha_{K,n}e^{-j\varphi_{K,n}}\mathbf{a}_{K,n}\end{bmatrix} \tag{19}$$

In multi-path environment, DBS generates a single beam directed toward each UE with uniform power allocation. However, CB generates multiple beams toward each UE in the directions of all paths with different beamforming power according to their channel gains as shown in (19).

Thus, SINR_k^{DBS} can be written as:

$$\text{SINR}_k^{DBS} = \frac{\left|\alpha_{k,1}\mathbf{a}_{k,1}^H\mathbf{a}_{k,1}+\sum_{n=2}^{N_k}\alpha_{k,n}e^{j\varphi_{k,n}}\mathbf{a}_{k,n}^H\mathbf{a}_{k,1}\right|^2}{\sum_{u=1,u\neq k}^{K}\left|\sum_{n=1}^{N_k}\alpha_{k,n}e^{j\varphi_{k,n}}\mathbf{a}_{k,n}^H\mathbf{a}_{u,1}\right|^2+\frac{\sigma_n^2}{\eta^{DBS}}} \tag{20}$$

And, SINR_k^{CB} can be written as:

$$\text{SINR}_k^{CB} = \frac{\left|\sum_{n=1}^{N_k}\alpha_{k,n}^2\mathbf{a}_{k,n}^H\mathbf{a}_{k,n}+\sum_{n=1,n\neq m}^{N_k}\sum_{m=1}^{N_k}\alpha_{k,n}\alpha_{k,m}e^{j(\varphi_{k,n}-\varphi_{k,m})}\mathbf{a}_{k,n}^H\mathbf{a}_{k,m}\right|^2}{\sum_{u=1,u\neq k}^{K}\left|\sum_{n=1}^{N_k}\sum_{m=1}^{N_u}\alpha_{k,n}\alpha_{u,m}e^{j(\varphi_{k,n}-\varphi_{u,m})}\mathbf{a}_{k,n}^H\mathbf{a}_{u,m}\right|^2+\frac{\sigma_n^2}{\eta^{CB}}} \tag{21}$$

In multi-path environment, for DBS, the interference factor is defined as $\beta_{k,u,n} = \mathbf{a}_{k,n}^H\mathbf{a}_{u,1}$. Thus the interference is due to the LOS beam $\mathbf{a}_{u,1}$ of UE_u ($\forall u \neq k$), that interferes with all the multi paths of UE_k, represented by $\mathbf{a}_{k,n}^H$. The interference is high if $\vec{\Theta}_{k,n}$ is close to $\vec{\Theta}_{u,1}$. Accordingly, even if all UEs are not located in the same direction, there is an interference coming from the non-LOS (NLOS) paths.

In case of CB, the interference factor is defined as $\beta_{k,u,n,m} = \mathbf{a}_{k,n}^H\mathbf{a}_{u,m}$. So the interference results from the collision of multiple beams $\mathbf{a}_{u,m}$ generated at each UE_u with all paths $\mathbf{a}_{k,n}^H$ of UE_k channel. It also depends on their channel gains as shown in (21).

Moreover, for DBS, the received power, observed at the numerator in (20), depends on the received power of the LOS path $\alpha_{k,1}\mathbf{a}_{k,1}^H\mathbf{a}_{k,1} = \alpha_{k,1}M$ plus the effect of paths in the vicinity of the LOS path, i.e., such that $\mathbf{a}_{k,n}^H\mathbf{a}_{k,1}$ is close to M. In contrast, for CB, the received power comes from the received power $\alpha_{k,n}^2\mathbf{a}_{k,n}^H\mathbf{a}_{k,n}$ for each path of UE_k plus the effect of paths that are close to each other. Here, we can conclude that DBS lacks the potentiality of NLOS paths contrary to CB, and loses some of the radiated energy.

IV. Numerical results

TABLE I: Simulation parameters

Parameters	Value
Carrier frequency	28 [GHz]
Channel bandwidth	20 [MHz]
Cell radius	100 [m]
Antenna separation distance	wavelength/2
Transmission power	30 [dBm]
Noise power	-100.9178 [dBm]

In this section, the performance of DBS and CB, in terms of sum-rate, is provided in urban mono- and multi-path environments. We assume that BS uses different AACs with 64 antennas: ULA, UPA with $M_H = 32$ and UPA with $M_H = 16$. System parameters used for performance assessment are listed in Table I. We consider perfect CSIT, i.e. perfect channel estimation at the receiver and perfect instantaneous channel feedback. The temporal and spatial parameters are generated using NYUSIM. The NYUSIM channel model is built based on extensive mmWave measurements in various outdoor urban and rural environments, and is developed using the time cluster-spatial lobe approach. NYUSIM generates distance and angles of each user according to statistical distributions. The sum-rate is averaged over 2000 channel realizations.

A. Mono-path environment

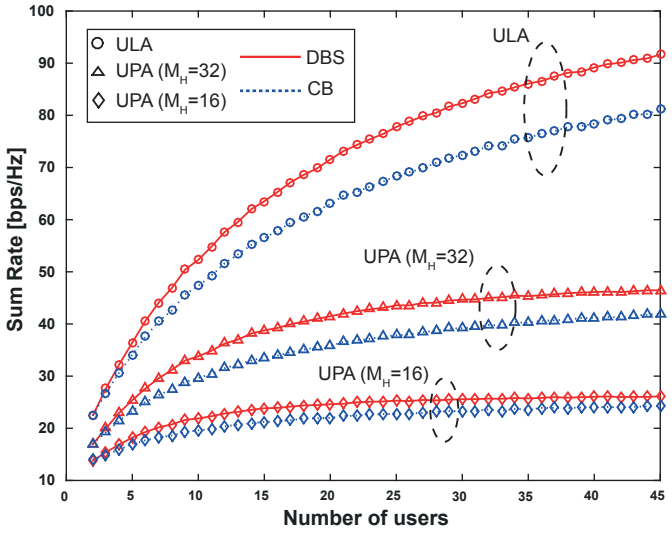

Fig. 2: Sum-rate achieved by mmWave m-MU-MIMO system using DBS and CB in mono-path environment.

In Fig. 2, the system sum-rate with either DBS or CB is presented as a function of the number of simultaneously served users in mono-path environment, with different AAC. This figure shows clearly that DBS outperforms CB in mono-path environment using either ULA or UPA.

In order to illustrate the spatial behavior of both beamformers, the spatial distribution on the xoy plane of five UEs served simultaneously by ULA array and their beam patterns, using DBS, are represented in Fig. 3 for two realizations. Moreover, it is worth noting as well that the beam patterns in Fig. 3 only give a view of the beamwidth and the steering direction, without any relation between the scale and the beam power. The first realization corresponds to the case where there is inter-user interference, whereas UEs are well separated from each other in the second realization. Moreover, the rate R_k and the channel gain α_k of UE$_k$ with $k = \{1, 2, 3, 4, 5\}$ are summarized in Table II.

In the first realization, as seen in Fig. 3a, UE$_1$ and UE$_4$ are not close to any other UEs, and therefore their rates are high, as seen in Table II, using both DBS and CB. For DBS, their rates are almost equal, while UE$_1$ has a greater rate than UE$_4$ for CB, since $\alpha_1 > \alpha_4$. UE$_2$ is located between UE$_3$ and UE$_5$. Actually, as UE$_5$ has the strongest channel gain, while UE$_2$ and UE$_3$ have weak channel gains, the rates R_2^{CB} (= 0.3) and R_3^{CB} (= 0.8) are very low whereas R_5^{CB} (= 10.5) is very high. For DBS, the inter-user interference significantly decreases the rate of UE$_5$, R_5^{DBS} (= 4.3).

In the second realization, UEs are well separated. From Table II, we can see that the rate of each UE is approximately the same when using DBS, whereas using CB, the higher the user channel gain is, the greater the achieved rate is.

In summary, these two realizations illustrate the fact that DBS gives a moderate rate for each UE independently of its channel gain, whereas CB reinforces the strong UEs and

TABLE II: System sum-rate, rate and channel gain of each UE for two different realizations where five UEs are served simultaneously with ULA in mono-path environment.

First realization					
metric	UE$_1$ (red)	UE$_2$ (green)	UE$_3$ (magenta)	UE$_4$ (blue)	UE$_5$ (yellow)
rate R_k^{DBS}	9.9	4.2	5.8	9.6	4.3
rate R_k^{CB}	9.8	0.3	0.8	8	10.5
channel gain α_k	2.3e-6	1.4e-7	5.6e-8	4.8e-7	1.1e-5
Sum-rate $R_{DBS} = 33.8$, $R_{CB} = 29.4$					
Second realization					
rate R_k^{DBS}	10.3	9.5	9.2	9.3	9.6
rate R_k^{CB}	10.1	7.5	8.4	10.7	10
channel gain α_k	3.5e-7	9.8e-8	3 e-7	7.5e-7	3.5e-7
Sum-rate $R_{DBS} = 47.9$, $R_{CB} = 46.7$					

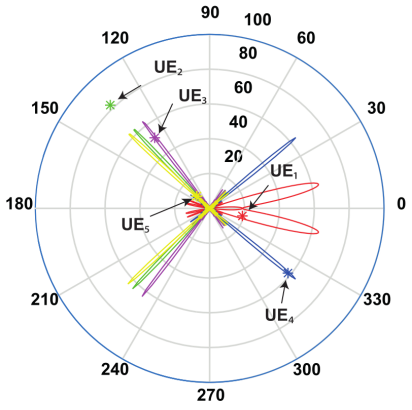

(a) First realization

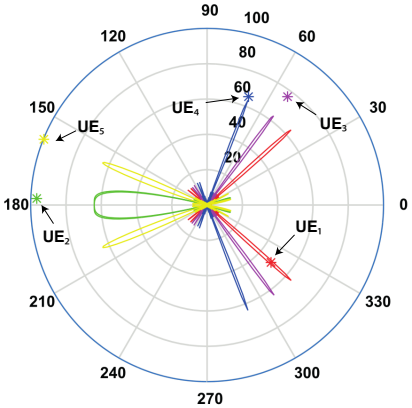

(b) Second realization

Fig. 3: Azimuth representation of the spatial distribution of UEs (*), on the xoy plane, with their ULA beam patterns, using DBS for the two realizations in mono-path environment. Each UE is illustrated by a colored * and its corresponding beam has the same color. Note that the scale corresponds to the separation distance between UEs and BS in meter, where BS is located at the center of the circle.

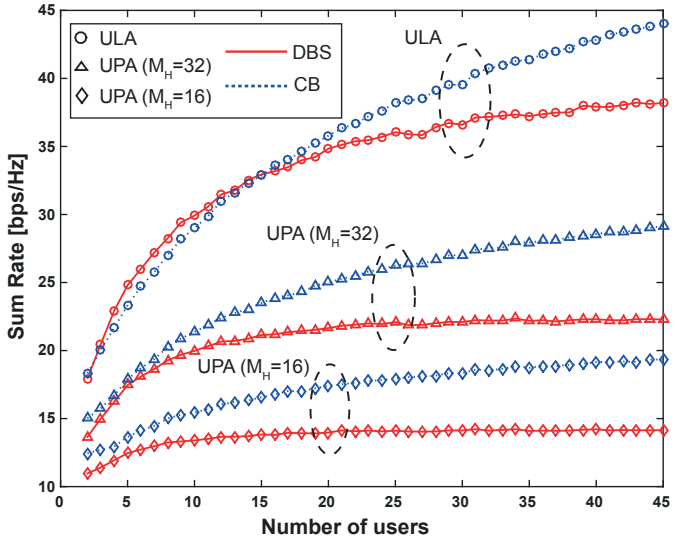

Fig. 4: Sum-rate achieved by mmWave m-MU-MIMO system using DBS and CB in multi-path environment.

marginalizes the weak UEs, as already explained in Section III-A.

B. Multi-path environment

In multi-path environment, the number of paths N_k in UE$_k$ channel follows a uniform distribution ranging from 2 to 30 as described in [9], and all paths belong to the same time-cluster (narrowband channel assumption).

In Fig. 4, the system sum-rate with either DBS or CB is presented as a function of the number of simultaneously served users in multi-path environment, with different AAC. We can see that the sum-rate R_T^{CB} is always larger than R_T^{DBS} when using UPA. However, when BS adopts ULA, DBS is better than CB as long as $K < 15$, and CB becomes better afterwards.

To illustrate the sum-rate results, seven UEs served simultaneously are considered by applying ULA and UPA ($M_H = 16$). For this realization and for each UE, the spatial distributions of paths, on the xoy plane, are represented in Fig. 5. The LOS path of each UE determines the direction of the UE position. This is corroborated by the spatial distributions of the seven UEs, on the xoy plane, represented in Fig. 6, with their beam patterns obtained by applying ULA and DBS. In Fig. 6, the same note, about scale and beam pattern, as in Fig. 3, is considered. The achievable rate of each UE is summarized in Table III.

First, as shown in Fig. 6, UEs are well separated in space. Therefore, since DBS generates a single beam toward each UE, these beams are also well separated. Second, when applying ULA with 64 antennas, the generated beams are very narrow, as shown in Fig. 6. Thanks to these narrow beams, on Fig. 5, we observe that, except for UE$_6$, the NLOS paths of each user weakly interfere with the other UE beams that are in the direction of user LOS path. Thus, with ULA, DBS provides interesting sum-rate as seen in Table III, with R_T^{DBS} (= 40.3) larger than R_T^{CB} (= 27.8). Similar results are shown in Fig. 4, where, DBS is better than CB as long as $K < 15$ with ULA.

TABLE III: Sum-rate and rate of each UE where seven UEs are served simulateneously by ULA or UPA and using either CB or DBS.

	ULA-R_k^{DBS}	ULA-R_k^{CB}	UPA-R_k^{DBS}	UPA-R_k^{CB}
UE$_1$ (red)	6.4	2.5	1.5	1.9
UE$_2$ (green)	4.1	2.6	3.1	2.4
UE$_3$ (magenta)	5.5	3.7	0.4	2.6
UE$_4$ (blue)	6	2.8	2.1	2
UE$_5$ (yellow)	9	5.7	5.3	4.8
UE$_6$ (black)	1.8	1.8	0.2	0.5
UE$_7$ (cyan)	7.5	8.7	2.5	7.5
Sum-rate	40.3	27.8	15.1	19.1

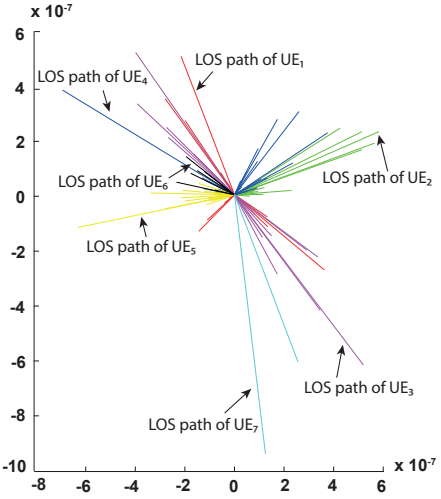

Fig. 5: Azimuth representation of the spatial distribution of paths, on the xoy plane, for one realization in multi-path environment. All paths belonging to the same UE channel are identified by the same color. The used scale corresponds to their channel gain.

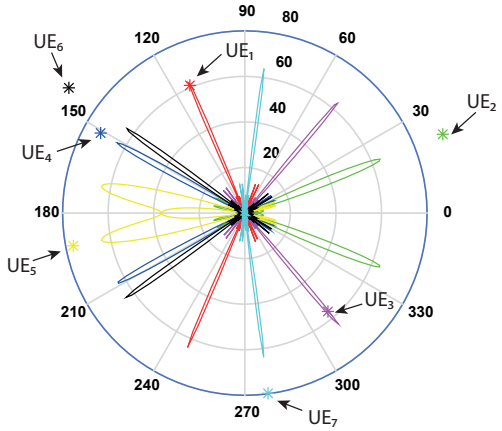

Fig. 6: Azimuth representation of the spatial distribution of UEs (*), on the xoy plane, with their ULA beam patterns, using DBS, for one realization. Each UE is illustrated by a colored * and its corresponding beam has the same color.

Let's now observe the performance of DBS when applying UPA instead of ULA, in Fig. 4. ULA provides the best

performance since its azimuthal resolution is able to discriminate the users spatially. With UPA, the number of horizontal antennas and so its azimuthal resolution decreases, creating more inter-user interference. For ULA, thanks to a narrow beam, the NLOS of UE_1 (red) do not interfere with the beam of UE_3 (magenta). However, for UPA, with wider beams, the interference increases and we observe a significant degradation of the rate from R_1^{DBS} (=6.4), for ULA, to R_1^{DBS} (=1.5), for UPA, as seen in Table III. The same explication holds for the significant degradation of rate for UE_3, UE_4 and UE_7, when using DBS and passing from ULA to UPA.

Obviously, there is also a degradation of the CB sum-rate when passing from ULA to UPA due to wider beamwidth. However, this degradation is less than that of DBS sum-rate, and thus CB outperforms DBS for UPA, as illustrated in Fig. 4. In Table III, R_T^{DBS} (= 15.1) is less than R_T^{CB} (= 19.1) when applying a UPA array with $M_H = 16$. This is mainly because DBS misses the potentiality of NLOS paths, while CB exploits their spatial diversity, as explained in Section III-B.

From Fig. 4, we can see that the sum-rate of DBS is flat from a certain value of K, depending on the number of horizontal antennas, i.e., the azimuth beamwidth. However, the sum-rate of CB still increases when more UEs are served simultaneously. Indeed, for DBS, first, if more UEs are served by BS, then more paths exist, and the interference coming from those paths (NLOS or LOS) increases. Second, DBS lacks the NLOS paths potentiality in terms of radiated energy.

The performance of classical beamformer such as zero forcing (ZF) that eliminates the inter-user interference, decreases at some point with an increasing number of UEs [14], while the sum-rate of both DBS and CB monotonously increase as shown in Fig. 2 and Fig. 4. Indeed, when more UEs are served simultaneously, ZF fails to eliminate the inter-user interference, and thus its performance degrades, while DBS and CB still achieve their goals.

V. Conclusion

In this paper, we considered multi-user digital beamforming in mmWave MIMO systems implemented by dozens of antennas. Unlike prior work, our evaluation is done using a realistic channel model generated by NYUSIM able to provide path angle information in an urban scenario. We first explored the theoretical derivation of sum-rate for DBS and CB in mono- and multi-path environments. Therefore, while relying on simulations based on geometric aspects, we have obtained the following results:

- In mono-path environment, DBS gives a moderate rate for each user, while CB reinforces the strong users and marginalizes the weak ones.
- In multi-path environment, for DBS, even when users are well separated in space, there is an interference coming from the NLOS paths. Besides, CB maximizes the BF gain by exploiting the diversity of NLOS paths whereas DBS lacks their potentiality and loses some of the radiated energy.
- The number of users, that DBS can serve simultaneously in multi-path channel, is constrained by the number of horizontal antennas, i.e., the azimuth beamwidth.

Finally, DBS is an appealing beamformer for mmWave massive MIMO systems in terms of complexity and channel feedback. However, it needs to be coupled to another interference management scheme to overcome its low performance when the number of users increases in the cell.

VI. Acknowledgment

This work has been funded by IMT Atlantique, Lebanese University and the AZM association.

The authors would like to thank Shihao Ju, Shu Sun and Theodore S. Rappaport of NYU Wireless, and New York University for providing open source simulator referenced as NYUSIM.

References

[1] T. S. Rappaport, S. Sun, R. Mayzus, H. Zhao, Y. Azar, K. Wang, G. N. Wong, J. K. Schulz, M. Samimi, and F. Gutierrez Jr, "Millimeter wave mobile communications for 5G cellular: It will work!" *IEEE access*, vol. 1, no. 1, pp. 335–349, 2013.

[2] E. G. Larsson, O. Edfors, F. Tufvesson, and T. L. Marzetta, "Massive mimo for next generation wireless systems," *IEEE Commun. Mag.*, vol. 52, no. 2, pp. 186–195, 2014.

[3] E. Bjornson, L. Van der Perre, S. Buzzi, and E. G. Larsson, "Massive mimo in sub-6 ghz and mmwave: Physical, practical, and use-case differences," *IEEE Wireless Commun.*, vol. 26, no. 2, pp. 100–108, 2019.

[4] R. W. Heath, N. Gonzalez-Prelcic, S. Rangan, W. Roh, and A. M. Sayeed, "An overview of signal processing techniques for millimeter wave mimo systems," *IEEE J. Sel. Topics Signal Process.*, vol. 10, no. 3, pp. 436–453, 2016.

[5] S. Hur, T. Kim, D. J. Love, J. V. Krogmeier, T. A. Thomas, and A. Ghosh, "Millimeter wave beamforming for wireless backhaul and access in small cell networks," *IEEE Trans. Commun.*, vol. 61, no. 10, pp. 4391–4403, 2013.

[6] S. Dutta, C. N. Barati, A. Dhananjay, D. A. Ramirez, J. F. Buckwalter, and S. Rangan, "A case for digital beamforming at mmwave," *arXiv preprint arXiv:1901.08693*, 2019.

[7] A. Rozé, M. Hélard, M. Crussière, and C. Langlais, "Millimeter-wave digital beamsteering in highly line-of-sight environments for massive MIMO systems," in *Wireless World Research Forum Meeting*, vol. 35, 2015.

[8] T. S. Rappaport, S. Sun, and M. Shafi, "Investigation and comparison of 3GPP and NYUSIM channel models for 5G wireless communications," in *Proc. IEEE Vehicular Technology Conference (VTC)*, 2017.

[9] M. K. Samimi and T. S. Rappaport, "3-D millimeter-wave statistical channel model for 5G wireless system design," *IEEE Trans. Microw. Theory Tech.*, vol. 64, no. 7, pp. 2207–2225, 2016.

[10] S. Sun, T. S. Rappaport, M. Shafi, P. Tang, J. Zhang, and P. J. Smith, "Propagation models and performance evaluation for 5G millimeter-wave bands," *IEEE Trans. Veh. Technol.*, vol. 67, no. 9, pp. 8422–8439, 2018.

[11] N. Fatema, G. Hua, Y. Xiang, D. Peng, and I. Natgunanathan, "Massive MIMO linear precoding: A survey," *IEEE Syst. J.*, no. 99, pp. 1–12, 2017.

[12] H. Yang and T. L. Marzetta, "Performance of conjugate and zero-forcing beamforming in large-scale antenna systems," *IEEE J. Sel. Areas Commun.*, vol. 31, no. 2, pp. 172–179, 2013.

[13] A. Alkhateeb, O. El Ayach, G. Leus, and R. W. Heath, "Channel estimation and hybrid precoding for millimeter wave cellular systems," *IEEE J. Sel. Topics Signal Process.*, vol. 8, no. 5, pp. 831–846, 2014.

[14] I. Khaled, A. El Falou, C. Langlais, B. ELHassan, and M. Jezequel, "Performance evaluation of linear precoding mmwave multi-user MIMO systems with NYUSIM channel simulator," in *Proc. IEEE Middle East and North Africa Communications Conference (MENACOMM)*, Nov. 2019.